International Journal of GEOMATE, May, 2025 Vol.28, Issue 129, pp.76-83
ISSN: 2186-2982 (P), 2186-2990 (O), Japan, DOI: https://doi.org/10.21660/2025.129.4891
Geotechnique, Construction Materials and Environment

COMPREHENSIVE EVALUATION OF FLEXURAL CAPACITY CALCULATION METHODS FOR ULTRA HIGH PERFORMANCE CONCRETE GIRDERS: EXPERIMENTS, SIMULATIONS, AND STANDARDS

Trung Hieu Tran[1], *Quoc Anh Vu[1] and Viet Chinh Mai[2]

[1]Faculty of Civil Engineering, Hanoi Architectural University, Vietnam
[2]Institute of Construction Technology, Le Quy Don Technical University, Hanoi, Vietnam

*Corresponding Author, Received: 24 Jan. 2025, Revised: 01 April 2025, Accepted: 02 April 2025

ABSTRACT: The current study evaluates the flexural capacity of Ultra High Performance Concrete (UHPC) girders through numerical simulations, experimental data, and existing design standards from the United States, France, and Switzerland. Finite element analysis (FEA) models are developed in Abaqus and calibrated against experimental results to ensure their reliability. A comparative analysis of 41 girders with varying strength, reinforcement ratios, fiber content, and cross-sectional dimensions is conducted to assess the loading capacity of different calculation methods. The findings indicate that numerical simulations predict flexural capacity with a standard deviation of 18.5% to 33% lower than design standards, demonstrating greater consistency with experimental data. Design standards generally provide more conservative predictions, ensuring safety margins for practical applications. These results highlight the potential for refining current calculation methods to achieve a balance between accuracy and safety in UHPC structural design.

Keywords: Ultra High Performance Concrete, Flexural capacity, Simulation method, Design code, CDP model

1. INTRODUCTION

Ultra high-performance concrete (UHPC), characterized by its tensile and compressive strengths, ductility, and durability, has properties that are superior to those of conventional concrete. These enhanced properties make UHPC an ideal material for structural applications requiring exceptional performance [1, 2]. Among the various structural elements, flexural girders are widely utilized in bridge structures, floor systems, and other construction projects where both flexural and shear resistance are critical requirements. The incorporation of steel fibers in UHPC further enhances its load-bearing capacity and crack resistance, improving its long-term structural integrity. Additionally, the superior bond between UHPC and reinforcement contributes to greater strain compatibility, allowing for more efficient force transfer within the girder system.

Numerous experimental studies have been conducted to investigate the flexural capacity of UHPC girders. Li et al. (2023) fabricated and tested five experimental specimens with varying amounts steel fiber [3]. The findings revealed that the ultimate loading capacity of the girders increased with higher fiber content, and the addition of steel fibers markedly improved shear capacity rather than flexural capacity. Girders with fiber content less than 2% exhibited shear failure, whereas specimens with fiber content of 2% or more experienced flexural failure. Qiu et al. (2020) conducted an experimental study on eight UHPC specimens to investigate the behavior of UHPC girders, focusing on crack shape and crack spacing in relation to the load-deflection curve [4]. The results showed that the crack width increased linearly with the applied load until the reinforcement yielded. As the applied load exceeded the yield threshold, one or two flexural cracks developed into dominant, large cracks. Yang et al. (2020) conducted a comparative study on the flexural behavior of UHPC girders and high-strength concrete girders [5]. A total of nine specimens were tested until failure. The results showed that the ductility factor of HSC girders decreased significantly as the reinforcement ratio increased, while the ductility factor did not exhibit a clear correlation with the reinforcement ratio. Singh et al. (2017) reported that the steel fibers in UHPC efficiently resisted crack propagation even after the yielding of tensile reinforcement, thereby improving the flexural capacity of the girders [6]. Several other noteworthy studies have investigated the flexural capacity of UHPC girders [7, 8].

Based on the literature review, it can be observed that previous studies exhibit limitations in terms of input parameters, due to high testing costs. Additionally, the influence of key parameters, such as fiber content, reinforcement ratio, and section geometry, on the flexural response of UHPC girders remains inadequately addressed. Conventional design codes, such as ACI 239C [9], AFNOR [10], and SIA [11], provide methodologies for estimating the flexural strength of UHPC girders. However,

these standards often adopt simplified assumptions that may not fully capture the nonlinear behavior and strain-hardening properties of UHPC, leading to the potential underestimation or overestimation of structural performance.

2. RESEARCH SIGNIFICANCE

This study aims to address the existing gaps in UHPC research by conducting a comprehensive evaluation and comparison of the flexural capacity of UHPC girders through experimental results, numerical simulations, and established design standards. The primary objectives of this research are: (1) to propose accurate numerical models for predicting the flexural response of UHPC girders; and (2) to assess the reliability and limitations of existing design codes in estimating flexural strength. The findings are expected to provide valuable insights for engineers and researchers in optimizing UHPC girder design, ultimately facilitating the broader adoption of this advanced material in modern infrastructure.

3. PRACTICE OF DESIGNING UHPC GIRDERS

This section predicts the flexural capacity of UHPC girders. The UHPC girder is selected from previous experimental studies. The loading capacity is calculated using various methods, including numerical simulations and design standards from the American, French, and Swiss codes. The results obtained from these approaches are then discussed and compared with test outcomes.

3.1 Input parameters of experimental analysis

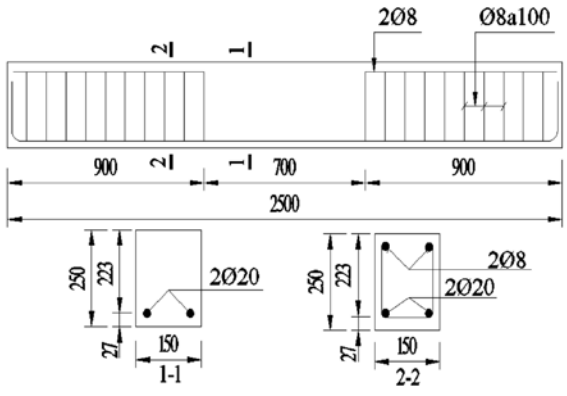

Fig. 1 Detail of the UHPC girders in the experiment by Umut Hasgul [12]

The experimental work by Umut Hasgul et al. to investigate the flexural capacity of UHPC girders is selected [12]. The girder features a cross-section of 150 × 250 mm and a length of 2500 mm. The tensile reinforcement consists of 2ϕ20 bars, with stirrups also arranged in this zone. The details of the experimental girder are illustrated in Fig. 1. The girder is subjected to a four-point bending test until failure. UHPC exhibits a compressive strength of 167 MPa, while the steel bars possess a yield strength of 463 MPa.

3.2 Numerical simulation analysis

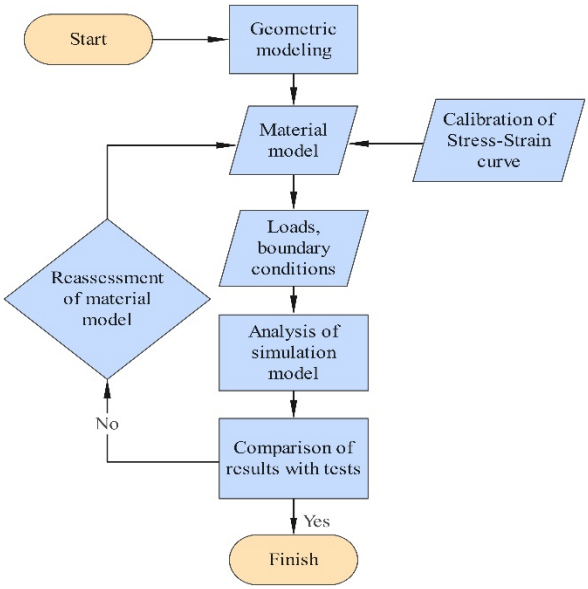

Fig. 2 Process of structural analysis through numerical simulation

The process of analyzing the UHPC girder using the numerical simulation method is shown in Fig. 2. The geometric parameters of the model serve as the foundational data, defining the girder span, cross-sectional dimensions, and longitudinal reinforcement arrangement. The material model is developed to represent the behavior of the UHPC in the simulation. To ensure that the model accurately reflects the experimental setting, the applied loads and boundary conditions are thoroughly implemented. A critical aspect of the simulation model build-up is the calibration of the UHPC stress-strain curve for the material model, which is described in the next section. Any significant inconsistencies between the simulation results and experimental data require the recalibration of the stress-strain curve. This iterative calibration procedure continues until the simulation results are highly reliable and consistent with the experimental results.

3.2.1 Material model

The Concrete Damaged Plasticity (CDP) model, which combines the theory of plasticity with fracture mechanics, is considered one of the most effective methods for simulating the nonlinear behavior of

concrete materials [13]. Due to its advantages, the CDP model was selected to simulate the behavior of the UHPC material in this study. The theoretical framework and formulation of the CDP model are extensively documented in the literature [14]. In Abaqus, the CDP model is executed using the following key parameters: the ratio of biaxial compressive strength to uniaxial compressive strength (σ_{bo}/σ_{co}), the shape parameter of the failure surface (Kc), the dilation angle (ψ), the eccentricity (ϵ), the viscosity parameter (μ), and the calibration stress-strain curve of UHPC [15]. Table 1 provides the parameters for the UHPC material in the numerical simulation [16].

Table 1. Material parameters of UHPC used in simulation model

Specific gravity (ton/m^3)	Compressive strength (MPa)	Elastic modulus (MPa)	Tensile strength (MPa)	Poisson's ratio
2.45	150	45000	9	0.2
ψ	ϵ	σ_{bo}/σ_{co}	K_c	μ
36^0	0.1	1.07	2/3	0.005

3.2.2 Calibration of the stress-strain curve for UHPC

The stress-strain relationship in tension and compression is critical for properly determining the mechanical behavior of UHPC material. To accurately characterize the initiation and propagation of cracks, as well as the failure state of the girder, it is imperative to establish the stress-inelastic strain curve of the material. The inelastic strain during compression can be calculated using the following equation [15]:

$$\varepsilon_c^{in} = \varepsilon_c - \varepsilon_{oc}^{el};\ \varepsilon_{oc}^{el} = \sigma_c / E \quad (1)$$

Where $\varepsilon_c^{in}, \varepsilon_c, \varepsilon_{oc}^{el}$ represent the inelastic strain, total strain, and elastic strain under compression at the point of interest; σ_c, E correspond to the compressive stress, and the elastic modulus derived from the stress-strain curve. Similarly, the cracking strain for tension can be obtained.

Based on these equations, the relation for inelastic stress-strain of UHPC under compression and tension are provided in Fig. 3. It is important to note that the curves derived from non-zero stress values. The initial point of the stress-inelastic strain curve corresponds to the endpoint of the linear phase in the respective curves. For UHPC materials, this initial point typically lies within 50–80% of the maximum compressive and tensile strength values. To generate curves with reliable data, it is essential to establish appropriate assumptions and perform iterative analyses of the model multiple times to validate the simulation outcomes against experimental results. Ultimately, for a compressive strength of 150 MPa and a tensile strength of 9 MPa, the initial stress values of the stress-inelastic strain curves in Fig. 3 are 110 MPa for compression (110/150 = 73%) and 5.8 MPa for tension (5.8/9 = 64.4%).

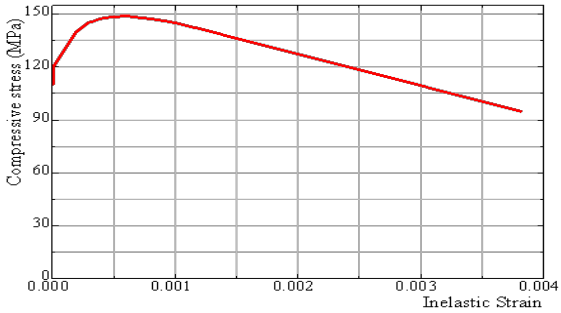

(a) Compression

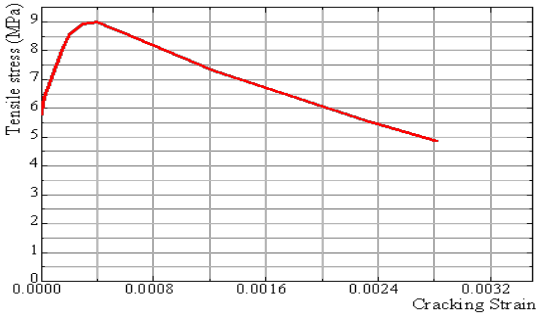

(b) Tension

Fig. 3 Stress-inelastic strain curves of UHPC after calibrating

3.2.3 Numerical simulation model

Based on the experimental investigation conducted by Umut Hasgul, the geometric representation and three-dimensional simulation model of the UHPC subjected to a four-point bending test were constructed, as shown in Fig. 4 [12].

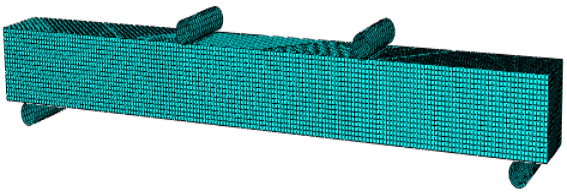

Fig. 4 Simulation mesh model of the UHPC girder

In the Abaqus model, the linearly reduced three-dimensional integrated element (C3D8R) is employed to simulate the concrete material [17]. For the reinforcement, a 3D linear bar element (T3D2) is applied, which accounts only for tensile and compressive stresses within the element. A convergence analysis is conducted with the mesh sizes of 20mm, 18mm, 15mm, and 12mm. While finer mesh sizes in the simulation model improve accuracy, they also significantly increase computational time. The 15mm mesh size is

selected, as it provides an optimal balance between model accuracy and computational efficiency, as shown in Fig. 4. The boundary conditions are implemented to match those of the simply supported girder in Umut Hasgul's experimental study, ensuring consistency between the numerical and experimental setups.

3.3 Flexural capacity of girder according to design standards

This section presents the procedure for assessing the flexural capacity of UHPC girders in accordance with the ACI 239C code [9]. Likewise, estimations based on other design standards, such as those established by France [10] and Switzerland SIA [11], are performed following similar procedures. Fig. 5 illustrates the stress-strain distribution of the UHPC girder. Input parameters for estimating the flexural capacity of the girders are listed in Table 2.

Table 2. Input parameters for estimating the flexural capacity of UHPC girders in accordance with ACI 239C [18].

Parameter	Unit	Value
Compressive strength f_c	MPa	167
Tensile strength f_t	MPa	10
Ratio of fiber length / diameter ($l_{f/\Phi}$)	mm	13/0.12
Fiber content v_f	%	2
Girder height h	mm	250
Girder width b	mm	150
Tensile reinforcement 2ϕ20	mm^2	628
Yield strength of steel	MPa	491

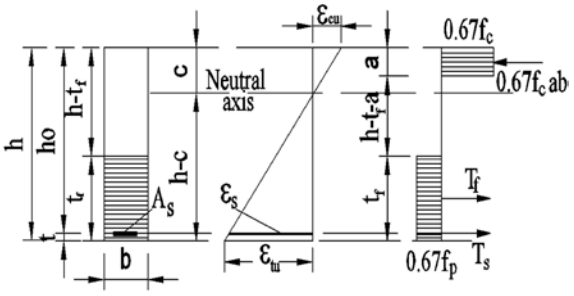

Fig. 5 Stress-strain distribution in UHPC girders in accordance with the ACI 239C [18]

The strength attributable to the fibers, known as the post-cracking strength f_p, depends on parameters such as the bond strength (τ_u), the fiber volume content v_f, the ratio of fiber length to diameter ($l_{f/\Phi}$), and coefficients (η_{lt}, η_{ot}) related to fiber dispersion within the matrix. The post-cracking strength can be determined using the following equations [18]:

$$f_p = 2\eta_{lt}\eta_{ot}v_f(l_f/\Phi)\tau_u \quad (2)$$

In most cases of fiber-reinforced concrete materials, including UHPC, steel fibers are generally utilized with lengths smaller than one of the girder's two primary dimensions: width or height. Under these conditions, the factors η_{lt}, η_{ot} are taken as 0.5 and 0.41, respectively [19]. The bond strength value, τ_u, is referenced as 4 MPa based on ACI Committee 544.1R [19]. The tensile strength, f_p, is determined using the following equation:

$$f_p = 1.64v_f(l_f/\Phi) \quad (3)$$

Given the reduction in the tensile strength of steel fibers as the crack width increases, a limitation on the tensile strain, ε_{tu}, is required. The value of ε_{tu} is influenced by the fiber length, l_f, and the crack spacing, S_{cr}, as described by the equation:

$$\varepsilon_{tu} = l_f/8S_{cr} \quad (4)$$

The crack spacing S_{cr} is expressed as (0.5-0.8)h, where h represents the height of the girder. For this study, S_{cr} is set at 0.5h=125 mm. Substituting this value, ε_{tu} is calculated as: ε_{tu} = 13/(8×125)=0.013

The maximum compressive strain of UHPC, ε_{cu} = 0.004, is derived from prior studies [12]. Applying the values ε_{tu} = 0.013 and ε_{cu} = 0.004, the neutral axis height, c, is determined to be 58.8 mm.

The coefficient b, which determines the height of the compression zone, is calculated using the following equation:

$$\{\beta = 1.05 - 0.05\times(f_c/6.9); 0.65 \le \beta \le 0.85 \quad (5)$$

Then the value of b is determined to be 0.65. Thus, the height of the compression zone is computed as: a = c × b = 58.8 × 38.2 mm.

The tensile force generated by the steel reinforcement, Ts, is calculated as: $T_s = A_s \times f_y$ = 628 × 491 = 308348 N = 308.3 kN

The height of the stress distribution, t_f, resulting from the steel fiber component, is governed by the coefficient ξ. This coefficient represents the ratio between the tensile to compressive strength and can be determined using the equation:

$$\xi = f_t/(f_c + f_t) = 10/(167 + 10) = 0.056 \quad (6)$$

Then, t_f = 0.67× (1-x)×h = 158.1 mm

The total force generated by the steel fiber component is obtained as follows:

$$T_f = f_p b t_f = 1,64 v_f(l_f/\Phi) b t_f = 84214\,N \quad (7)$$

The flexural capacity, Mn, is determined by applying the moment equilibrium equation about the central axis of the compression zone:

$$M_n = T_s(h_0 - \beta c/2) + T_f[h - (t_f + \beta c)/2] \quad (8)$$

By substituting the values into the equation, the flexural capacity is calculated as: M_n =75.65×10^6 N.mm. Under the same procedure, the flexural capacity of UHPC girders is also evaluated in accordance with the French and Swiss standards. The subsequent section presents and discusses the comparative analysis of the results generated by these approaches.

4. RESULTS AND DISCUSSION

Fig. 6 shows the load-deflection curve for the UHPC girder under the four-point bending test, derived from both the experimental study by Umut Hasgul and the numerical simulation [12]. The load-deflection curves from Umut Hasgul's test and the simulation exhibit similar trends, consisting of four stages: elastic stages, nonlinear stage, plasticity stage and failure. The load-deflection curve derived from the numerical simulation demonstrates a smoother and more stable trend compared to the experimental results, which exhibit greater variations likely due to material imperfections and testing conditions. As shown in Table 3, the maximum difference in the load values between the simulation and experimental results is 8%, indicating a good agreement between two approaches.

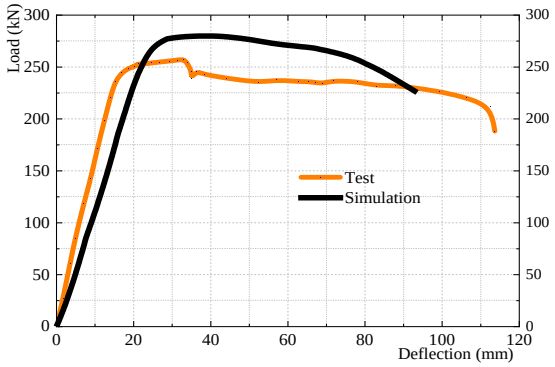

Fig. 6 Load-deflection curve of the UHPC girder from Umut Hasgul's test and the numerical simulation

Table 3. Maximum applied load on the UHPC girder according to the test and the simulation

Case study	Maximum loading (kN)	Disparity (T/S)
Test (T)	257.51	//
Simulation (S)	279.86	0.92

Fig. 7 illustrates the crack propagation in the UHPC girder as observed in both the simulation and experimental results. As shown in Fig. 7a, the initial cracks appear beneath the point load positions. As the applied load increases, the quantity, length, and width of the cracks correspondingly increase, as illustrated in Fig. 7b. Fig. 7c and 7d presents a comparison of the failure patterns of girder at the maximum applied load between the simulation and the experiment. At this stage, the girder displays significant deformation. A prominent crack develops at the mid-span of the girder, characterized by a large width and an upward progression toward the compression zone. This observation closely aligns with the experimental failure mode. These findings demonstrate that the simulation model exhibits high reliability and agrees well with the experimental results.

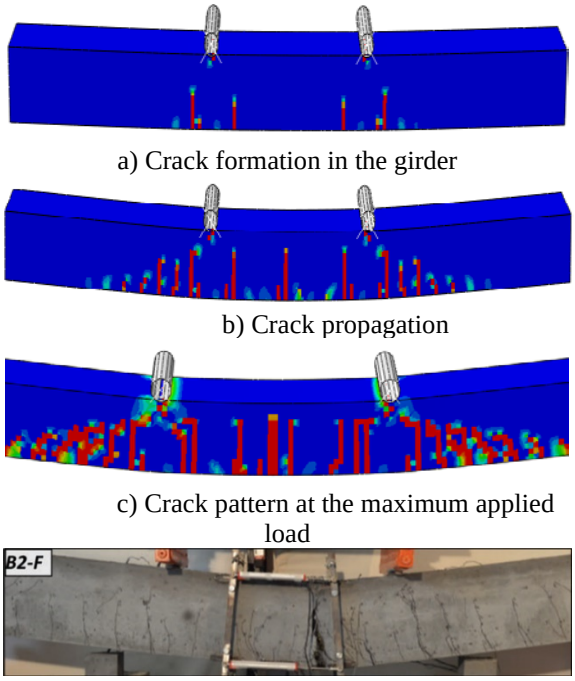

a) Crack formation in the girder

b) Crack propagation

c) Crack pattern at the maximum applied load

d) Crack pattern in the UHPC girder by the test of Umut Hasgul [12]

Fig. 7 Crack pattern of the UHPC girder in simulation (a, b, c) and the test of Umut Hasgul (d)

Table 4. Maximum flexural capacity (kN·m) according to various approaches

Case study	Test	Simulation	ACI	AFNOR	SIA
Loading capacity (kN.m)	89.76	97.55	75.65	78.1	77.4
Disparity compared to the test	//	0.92	1.19	1.15	1.16

Table 4 provides a summary of the bending capacity of UHPC girders determined by various methods, including the experimental data [12], numerical simulation, and estimations based on the American (ACI 239C) , French (AFNOR), and Swiss (SIA) standards. Comparing the bending capacity obtained from these methods with the test results reveals that the simulation method achieves the closest match, with a difference of only 8%. Calculations based on American, French, and Swiss standards yield larger disparities of 19%, 15%, and 16%, respectively. Based on the validated numerical simulation model and the standard-compliant estimation methods, the calculation range was expanded by employing 41 girder samples with the different parameters. These girders feature a range of cross-sectional dimensions, with widths ranging

from 15 cm to 20 cm and heights ranging from 22 cm to 38 cm. The UHPC material has fiber volume contents of 1.0%, 1.5%, and 2.0%, respectively. The steel reinforcement ratio (ρ) varies between 0% and 1.96%. The minimum compressive strength of UHPC is 126 MPa, while the yield strength of steel ranges from 412 MPa to 523 MPa.

Table 5 and Fig. 8 present the comparative analysis of the UHPC flexural capacity determined through various methods. Results obtained from the tests (T) range from 39.3 kN.m to 171.2 kN.m, while the values from simulation (S) range from 33.4 kN·m to 159.5 kN·m. The test/simulation (T/S) ratio varies between 0.85 and 1.18. Compared to the estimations proposed by the ACI, AFNOR, and SIA standards, the numerical simulation provides the predictive model that most closely aligns with the experimental results. Most simulated values are slightly higher than the experimental ones, which can be attributed to the idealized conditions assumed in numerical simulations, particularly in material behavior and loading conditions. The ratio of test to ACI (T/ACI) fluctuates from 0.87 to 1.30, indicating that, in some cases, the ACI standard provides results closer to the experiments than the AFNOR and SIA standards. The ACI standard tends to underestimate the bearing capacity, aligning with the safety principles inherent in structural design. The ratio of test to AFNOR (T/AFNOR) and test to SIA (T/SIA) ranges from 0.87 to 1.31 and 0.86 to 1.32, respectively, reflecting a balance between safety and practicality. Most calculations based on these standards yield more conservative estimates of bearing capacity than the experimental results. Key factors such as cross-sectional geometry, reinforcement ratio, and fiber content significantly influence the outcomes, but the numerical simulation model has demonstrated relatively accurate predictive capabilities.

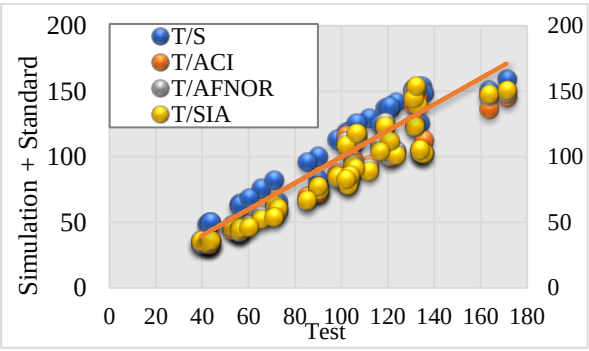

Fig. 8 Comparison of UHPC loading capacity (kN.m) predicted by various methods with experimental results

Fig. 8 depicts the distribution of results calculated by different methods compared to experimental data. The standard deviations for simulation, ACI, AFNOR, and SIA methods are 0.097, 0.115, 0.129, and 0.12, respectively. Standard deviation serves as a measure of variability with a higher standard deviation indicating greater data dispersion. The simulation method exhibits a more consistent T/S ratio than estimations derived from the standards, underscoring its applicability in design practice. Among the standards, ACI demonstrates greater alignment with experimental results compared to AFNOR and SIA. Additionally, the ACI code offers greater flexibility in predicting the loading capacity of UHPC girders, making it suitable for scenarios that demand more realistic and practical estimates compared to the AFNOR and SIA standards.

5. CONCLUSION

This study compares the flexural capacity of UHPC girders using various approaches, including experiments, numerical simulations, and design standards. Based on the findings, the following conclusions can be drawn:

- The numerical simulation method, calibrated with experimental results, demonstrates its potential as a highly reliable tool for predicting the flexural capacity of UHPC girders. Most simulated results are slightly higher than the test results. The lower standard deviation (18.5% to 33% less than design standards) confirms its reliability with test findings.
- The flexural capacity of UHPC girders predicted by the ACI, AFNOR, and SIA standards provides conservative results, with most of them being lower than the test outcomes. Conservative characteristics of the design standards aligns with safety principles in structural engineering. However, their inability to predict certain behaviors (e.g., crack initiation and propagation) limits their application for advanced structural design.
- In comparison to the AFNOR and SIA standards, the ACI design code generates outcomes that are more closely aligned with experimental findings. This makes ACI more applicable for scenarios where balancing safety with practicality is crucial.
- Combining numerical simulations with design standards offers a pathway to optimizing the design process. Simulations refine initial estimates, enabling designers to achieve more efficient, realistic, and reliable structural solutions.

Future research direction: Further investigations should focus on integrating more diverse loading conditions, varying environmental factors, and fatigue analysis to expand the applicability of numerical simulations and refine design standards. Experimental studies on non-standard UHPC applications are also essential to bridge gaps in current design methodologies.

Table 5 Comparison of calculations results for UHPC bending capacity using various methods

Reference	No.	Test - T (kN.m)	Simulation - S (kN.m)	T/S	ACI (kN.m)	T/ACI	AFNOR (kN.m)	T/ AFNOR	SIA (kN.m)	T/SIA
Qiu et al. (2020) [4]	B-S65-16	65.5	75.8	0.86	54.3	1.21	55.9	1.17	52.4	1.25
	B-S81-20	105	108.9	0.96	98.5	1.07	94.5	1.11	92.7	1.13
	B-S83-20	101.9	118.7	0.86	116.9	0.87	111.7	0.91	109.1	0.93
	B-H65-20	133	150.6	0.88	145.4	0.91	152.3	0.87	139.8	0.95
Hasgul et al. (2018) [12]	B1-F	52.6	48.3	1.09	44.2	1.19	46.4	1.13	47.1	1.12
	B2-F	89.8	97.6	0.92	75.7	1.19	78.1	1.15	77.4	1.16
	B3-F	111.9	129.3	0.87	93.8	1.19	91.6	1.22	89.1	1.26
	B4-F	134.4	154.1	0.87	106.3	1.26	102.8	1.31	103.4	1.30
Chen et al. (2018) [20]	B1	43.3	50.1	0.86	33.9	1.28	34.2	1.27	35.2	1.23
	B2	71.4	65.9	1.08	60.2	1.19	63.3	1.13	63.4	1.13
	B3	90.4	77.8	1.16	72.5	1.25	75.1	1.20	74.9	1.21
	B4	105.9	121.9	0.87	94.8	1.12	92.4	1.15	91.1	1.16
Yoo et al. (2017) [21]	UH-N	72.5	65.6	1.11	59.8	1.21	58.8	1.23	60.6	1.20
	UH-0.53	97.9	113.1	0.87	87.2	1.12	83.7	1.17	85.2	1.15
	UH-1.06	118.8	137.5	0.86	122.6	0.97	126.5	0.94	123.5	0.96
	UH-1.71	131	151.7	0.86	140.6	0.93	150.1	0.87	144.8	0.90
Yoo and Yoon (2015) [22]	S13-0.94	39.3	33.4	1.18	35.3	1.11	36.5	1.08	35.9	1.09
	S13-1.50	55.8	63.4	0.88	44.5	1.25	42.8	1.30	43.9	1.27
	S19.5-0.94	42	48.5	0.87	33.7	1.25	34.4	1.22	35.3	1.19
	S19.5-1.50	56.3	64.7	0.87	44.1	1.28	43.6	1.29	45.7	1.23
	S30-0.94	43.2	49.2	0.88	33.8	1.28	34.3	1.26	35.5	1.22
	S30-1.50	56.1	63.4	0.88	44.9	1.25	43.2	1.30	45.6	1.23
	T30-0.94	43.5	50.3	0.86	36.3	1.20	34.8	1.25	36.6	1.19
	T30-1.50	60.3	68.7	0.88	48.4	1.25	47.9	1.26	46.7	1.29
Meade and Graybeal (2010) [23]	S1-1	102.9	115.6	0.89	79.2	1.30	80.6	1.28	78.6	1.31
	S1-2	103.5	119.8	0.86	83.5	1.24	82.2	1.26	86.1	1.20
	S1-3	121	137.3	0.88	99.9	1.21	100.5	1.20	104.7	1.16
	S1-4	123.5	141.9	0.87	104.3	1.18	104.3	1.18	101.3	1.22
	S1-5	135.5	148.7	0.91	112.4	1.21	103.2	1.31	102.7	1.32
	S2-0	90	83.2	1.08	73.5	1.22	75.9	1.19	77.6	1.16
	S2-1	133.8	125.7	1.06	104.7	1.28	105.2	1.27	105.6	1.27
	S2-2	120.7	138.3	0.87	108.5	1.11	104.2	1.16	111.8	1.08
	S2-3	163.4	150.8	1.08	136.7	1.20	146.3	1.12	147.7	1.11
	S2-4	132.3	153.2	0.86	140.3	0.94	151.6	0.87	153.8	0.86
	S2-5	171.2	159.1	1.08	145.8	1.17	149.2	1.15	150.7	1.14
Yang et al. (2010)a [24]	NR-1,2	71	82.2	0.86	58.1	1.22	55.8	1.27	54.3	1.31
	NR12-1,2	85.1	96.4	0.88	69.9	1.22	66.6	1.28	66.7	1.28
	R13-1,2	102	111.5	0.91	84.7	1.20	85.5	1.19	82.9	1.23
	R14-1,2	116.7	124.9	0.93	110.6	1.06	108.7	1.07	104.4	1.12
	R22-1,2	106.4	125.7	0.85	114.5	0.93	116.1	0.92	118.2	0.90
	R23-2	131.6	146.1	0.90	125.4	1.05	122.8	1.07	123.5	1.07
Standard deviation			38.00	0.097	35.01	0.115	36.35	0.129	35.60	0.120

6. REFERENCES

[1] Yoo D. Y., Banthia N., and Yoon Y. S., Recent development of innovative steel fibers for ultra-high-performance concrete (UHPC): A critical review, Cement and Concrete Composites, Vol. 145, 2024, pp.105359.

[2] Dahish H.A. and Bakri M., Flexural Behavior of Rc Composite Beams With Ultrahigh Performance Fiber Reinforced Concrete Layer Using Finite Element Modeling, International Journal of GEOMATE, Vol. 22, Issue 93, 2022, pp. 75–82.

[3] Li J., and Yan J., Experimental and Numerical Study on the Mechanical Performance of Ultra-High-Performance Concrete T-Section Beams, Sustainability, Vol. 15, Issue 12, 2023, pp. 9849.

[4] Qiu M., Shao X., Zhu Y., and Wang Y., Experimental investigation on flexural cracking behavior of ultra high performance concrete beams, Structural Concrete, Vol. 21, Issue 5, 2020, pp. 2134–2153.

[5] Yang I. H., Park J., Bui Q., Kim C. and, Lee H., An Experimental Study on the Ductility and Flexural Toughness of Ultra High Performance Concrete Beams Subjected to Bending, Materials, Vol. 13, Issue 10, 2020, pp. 2225.

[6] Singh M., Sheikh A. H., and Griffith M.C., Experimental and Numerical Study of the Flexural Behaviour of Ultra-High Performance Concrete Beams, Construction and Building Materials, Vol. 138, 2017, pp. 12–25.

[7] Zhang W., Zheng D., Huang Y., and Kang S., Experimental and Simulative Analysis of Flexural Performance in UHPC-RC Hybrid Beams, Construction and Building Materials, Vol. 436, 2024, pp. 136889.

[8] Li Y., and Aoude H., Effect of high-strength and stainless steel reinforcement on the flexural behavior of UHPC beams, Case Studies in Construction Materials, Vol. 20, 2024.

[9] ACI 239C – Structural Design of UHPC, American Concrete Institute, 2015.

[10] AFNOR - Design of concrete structures: Specific rules for ultra-high performance fibre-reinforced concrete (UHPFRC) (NF P18-710), 2016.

[11] Swiss Society of Engineers and Architects (SIA), Recommendation: Ultra-high performance fibre-reinforced cement based composites (UHPFRC) construction material, dimensioning, and application, SIA, Lausanne, Switzerland, 2016.

[12] Hasgul U., Turker K., Birol T., and Yavas A., Flexural Behavior of Ultra‐High‐Performance Fiber Reinforced Concrete Beams With Low and High Reinforcement Ratios, Structural Concrete, Vol. 19, Issue 6, 2018, pp. 1577‐1590.

[13] Minh H. L., Khatir S., Wahab A., and Thanh L., A Concrete Damage Plasticity Model for Predicting the Effects of Compressive High-Strength Concrete Under Static and Dynamic Loads, Journal of Building Engineering, Vol. 44, 2021, pp. 103239.

[14] Lubliner J., Fenves L., A Plastic-Damage Model for Concrete, International Journal of Solids and Structures, Vol. 25, Issue 3, 1989, pp. 299–326.

[15] Dassault Systèmes, Abaqus/CAE User's Guide.

[16] Bahij S., Adekunle K., Al‐Osta M., Ahmad S., Al‐Dulaijan S., and Rahman M., Numerical Investigation of the Shear Behavior of Reinforced Ultra‐High‐Performance Concrete Beams, Structural Concrete, Vol. 19, Issue 1, 2018, pp. 305‐317.

[17] Khassaf S.I., Chkheiwr A., and Jasim M.A., Effect of Contraction Joints on the Structural Performance of Arch Dam, International Journal of GEOMATE, Vol. 19, 2020, pp. 219–227.

[18] Graybeal B.A., ACI 239C – Structural Design of UHPC, 2018.

[19] ACI Committee 544, ACI 544.1 R-96 – State of the Art: Report on Fibre Reinforced Concrete, ACI, Farmington Hills, MI, USA, 2002.

[20] Chen S., and Wang J., Flexural Behaviour of Rebar-Reinforced Ultra-High-Performance Concrete Beams, Magazine of Concrete Research, Vol. 70, Issue 19, 2018, pp. 997–1015.

[21] Yoo D. Y., Banthia N., and Yoon Y. S., Experimental and Numerical Study on Flexural Behavior of Ultra-High-Performance Fiber-Reinforced Concrete Beams With Low Reinforcement Ratios, Canadian Journal of Civil Engineering, Vol. 44, Issue 1, 2017, pp. 18–28.

[22] Yoo D. Y. and Yoon S., Structural Performance of Ultra-High-Performance Concrete Beams With Different Steel Fibers, Engineering Structures, Vol. 102, 2015, pp. 409–423.

[23] Meade T. and Graybeal B., Flexural Response of Lightly Reinforced Ultra-High Performance Concrete Beams, in Proc. Third Int. fib Congress and PCI Convention, Washington, DC, 2010.

[24] Yang I.H., Joh C., and Kim B.-S., Structural Behavior of Ultra High Performance Concrete Beams Subjected to Bending, Engineering Structures, Vol. 32, Issue 11, 2010, pp. 3478–3487.